J Mol Model (2010) 16:9–16
DOI 10.1007/s00894-009-0517-y

ORIGINAL PAPER

Bonding and electronic structures in W@Au_{12}AE complexes (AE= NO^+, CO, BF, CN^-, or BO^-): analogies among ligands isoelectronic to carbon monoxide

Yi Fu · Jia Li · Shu-Guang Wang

Received: 12 January 2009 / Accepted: 6 March 2009 / Published online: 23 May 2009

Abstract A theoretical study on the geometries and electronic structures of W@Au_{12}AE (AE=NO^+, BF, CN^-, or BO^-) was carried out to gain insight into interactions between W@Au_{12} and ligands isoelectronic with CO. The best configuration for the adsorption site is on-top type for all five complexes. After complexing with boron ligands (BF or BO^-), the axial Au–W bond distance in W@Au_{12} is lengthened notably, but NO^+ has the opposite effect on the axial Au–W bond. A charge transfer and energy decomposition analysis shows that the metal–ligand bonds have enhanced σ-donation strength from NO^+ to BO^-. Furthermore, the A–E bond strength in the complexes becomes weaker with stronger π-back-donation interactions. Finally, W@Au_{12}CO has the largest HOMO–LUMO gap, making it the most stable in terms of kinetic stability.

Keywords Density functional · Gold cluster · Closed-shell · Back donation

Introduction

Gold catalysis has emerged as one of the most attractive research areas in chemistry [1, 2]. One of the first breakthroughs was the discovery of the catalyzed hydrogenation of olefines reported by Bond et al. [3]. Later, Haruta et al. investigated the low temperature CO combustion [4, 5], followed by other catalyzed reactions such as propylene epoxidation [6] and NO_x reduction/dissociation [7]. In low temperature CO oxidation, smaller Au nanoparticles deposited on metal oxides, such as $Mg(OH)_2$, Al_2O_3, TiO_2 and SiO_2, show higher CO oxidation catalytic activity. In particular, Au/$Mg(OH)_2$, which contains a icosahedral Au_{13} cluster, has extremely high CO oxidation catalytic activity [8].

Studies have shown that preferential formation of Au_n clusters with n=13, 55, or 147 indicates that they are relatively stable compared to other-sized clusters [9–11]. The most plausible explanation for their marked stability is the intrinsic stability of the Au cores arising from closing of geometrical and/or electronic shells. Despite the fact that the bare 13-atom gold cluster has been shown not to possess a high-symmetry icosahedral structure, Pyykkö and Runeberg recently predicted a series of highly stable gold clusters containing an Au_{12} cage and a central heteroatom, M@Au_{12} (M = Ta^-, W, Re^+), which is isoelectronic to the known I_h Au_{13}^{5+} cage [12]. These remarkable M@Au_{12} clusters were shown to attain their stability from strong relativistic effects [13], aurophilic attraction [14], and perfect 18-electron counting [15, 16]. Shortly thereafter, the experimental observation and characterization of a series of icosahedral cage clusters was reported by the group of Lai–Sheng Wang [17]. Therefore, we chose to examine W@Au_{12}, which is the smallest cluster with inner atoms, as a first step towards understanding the catalytic activities of Au catalysts using quantum-chemical calculations.

Nowadays, diatomics isoelectronic to CO are quite well known in metal compounds. Studies comparing ligands isolobal to CO, such as N_2, NO^+, BF and CN^-, have been carried out [18–22]. The CO ligand is still thought to have unique versatility because of its special orbital electronic structure, which provides substantial intrinsic stability. However, the fact that AE (AE=NO^+, BF, CN^-, etc.) and

Y. Fu · J. Li · S.-G. Wang (✉)
School of Chemistry and Chemical Technology,
Shanghai Jiao Tong University,
200240 Shanghai, China
e-mail: sgwang@sjtu.edu.cn

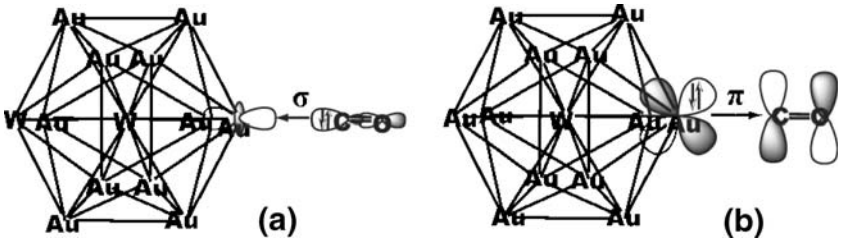

Fig. 1 **a** Schematic representation of the W@Au_{12}←CO σ–donation interaction. **b** W@Au_{12}←CO π-back-donation interaction

CO molecules are valent isoelectronic suggests that auro–AE can be used as a model system to provide further insights into the mechanisms of CO chemisorption on nanogold and nanogold catalytic properties.

In this paper, we will shed light on the interaction between CO and W@Au_{12}. Research has shown that the different electronic states of a complex play an important role in catalytic activity, and experiments indicate the existence of negatively charged Au atoms on an Au/TiO_2 catalyst [F. Boccuzzi, personal communication] and positively charged Au atoms on an Au/CeO_2 catalyst [23]. Thus, in addition to W@Au_{12}CO, ligands isoelectronic to CO, *AE* = NO^+, BF, CN^-, or BO^-, varying from cationic to neutral and anionic, were selected for comparison to investigate how the respective effects of negative and positive charges on ligands can influence the model.

Methods

Computational details

All calculations were performed at the density functional theory (DFT) level as implemented in the Amsterdam DFT package (ADF 2005), which was developed by Baerends et al. [24, 25]. The DFT method involves local density approximation (LDA), with the parameterization developed by Vosko et al. [26]. The nonlocal DFT level of theory uses gradient corrections to the exchange and correlation potentials developed by Perdew and Wang (PW91) [27, 28], respectively. In addition, relativistic effects were considered using the scalar and spinor relativistic zero–order regular approximation (ZORA) [29–32]. The valance electrons of all atoms were calculated using Slater-type-orbital (STO) basis sets of triple-ξ quality plus two polarized functions [33]. In order to save computing time, the inner shells of the atoms were calculated by the Dirac method [34] and then kept frozen during molecular calculations. The valence shells were taken as 2s, 2p and 5s, 5p, 5d, 6s for the second row elements and sixth row transition metals, respectively. Finally, charge analysis was performed with Weinhold's natural bond orbital (NBO) method [35–40] using the Gaussian 03 program [41].

The bond energy (BE) between metal fragment W@Au_{12} and AE ligands is defined as the energy needed to break the metal–ligand bonds. It can be divided into two physical components:

$$\mathrm{BE}(\mathrm{W@Au_{12}} - \mathrm{AE}) = -\left(\Delta E_{\mathrm{prep}} + \Delta E_{\mathrm{int}}\right) \quad (1)$$

Term ΔE_{prep} is the preparation energy for distortion of the fragments from their ground state equilibrium geometries to the geometries adopted upon complexation. It is calculated as

$$\Delta E_{\mathrm{prep}} = E_{\mathrm{W@Au12}}(\mathrm{in\ W@Au_{12}AE}) - E_{\mathrm{W@Au12}} + E_{\mathrm{AE}}(\mathrm{in\ W@Au_{12}AE}) - E_{\mathrm{AE}} \quad (2)$$

Term ΔE_{int} is the instantaneous interaction energy caused by the interaction of two fragments. According to the extended transition state (ETS) method initially

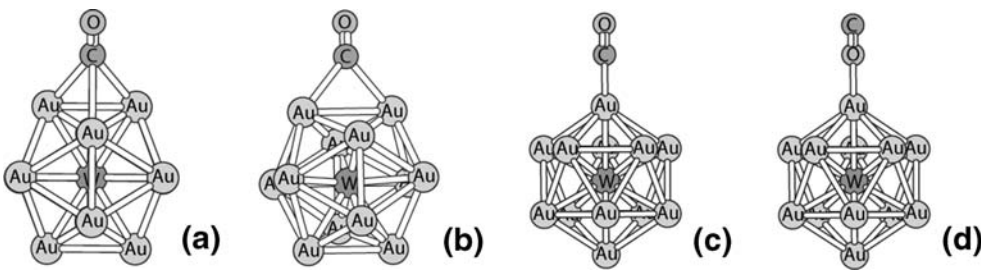

Fig. 2 **a–d** Calculated model structures of W@Au_{12}–AE. **a** Hollow type, **b** bridge type, **c** on-top type, **d** on-top type

Table 1 Bond energies (in kcal mol^{-1}) of W@Au_{12}AE (AE=NO^+, CO, BF, CN^-, or BO^-) with hollow, bridge or on-top configurations and on-top sited W@Au_{12}EA

AE	NO^+	CO	BF	CN^-	BO^-
Hollow	68.79	0.38	21.23	32.59	52.46
Bridge	66.05	–8.59	32.79	44.63	63.63
On-top	88.18	29.22	51.65	76.2	91.59
W@Au_{12}–EA (on-top)	41.16	1.08	0.53	59.02	42.38

developed by Ziegler and Rauk [42–44], it has the following main contributions:

$$\Delta E_{int} = \Delta E_{st} + \Delta E_{orb} = \Delta E_{pauli} + \Delta E_{elstat} + \Delta E_{orb} \quad (3)$$

ΔE_{st} is the steric interaction term [45–47] that represents the interaction energy between the two prepared fragments with the electron densities that each fragment would have in the absence of the other fragment. It summarizes the quasiclassical electrostatic interaction ΔE_{elstat} and the repulsive Pauli repulsion ΔE_{pauli}. Finally, the orbital interaction term, ΔE_{orb}, represents the stabilization produced when the Kohn–Sham orbitals relax to their optimal form.

The orbital metal–ligand interaction can be classically viewed as synergistic, where carbon monoxide acts simultaneously as σ–donor and π–acceptor. The bonding model is shown in Fig. 1 by Dewar's orbital interaction scheme [48]. In the present work, ΔE_{orb} can be partitioned into ΔE_σ and ΔE_π with respect to the different irreducible representations that are generated by the C_{5v} symmetry (on-top sited complexes) of the orbital. The C_{5v} group gives A_1, A_2, E_1 and E_2 irreducible representations. The orbital interaction contributions corresponding to σ–donation (Fig. 1a) come mainly from ΔE_{A1}, and π-back-donation (Fig. 1b) comes mainly from ΔE_{E1}. A small part also comes from ΔE_{A2} and ΔE_{E2}, due to neither σ nor π bonding but as a consequence of polarization by ligands.

Results and discussion

Adsorption sites of W@Au_{12}AE (AE=NO^+, CO, BF, CN^-, or BO^-)

The model W@Au_{12} cluster chosen was an icosahedral (I_h) fragment, which is more stable than a cuboctahedral (O_h) structure [49]. Various types of adsorption sites were probed by the five ligands: hollow, bridge and on-top positions at the cluster surface. During the optimization process, the on-top sited W@Au_{12}AE (AE=NO^+, CO, BF, CN^-, or BO^-) models always maintained C_{5v} symmetry, the bridge-sited ones had C_{2v} symmetry and the hollow sites C_{3v}. In addition to W@Au_{12}–AE, we also considered W@Au_{12}–EA with on-top configuration in order to specify whether the ligating atom was A or E. Figure 2 shows the optimized geometries for the AE ligand on the W@Au_{12} cluster. Table 1 summarizes the calculated bond energies of various adsorption geometries. From the results in Table 1, we found that the predominant form of binding for all five ligands is on-top, since adsorptions in the on-top configuration have the largest bond energies. Moreover, according to the bond energies, nitrogen, carbon and boron should be the atoms that link directly to the metal cluster. In the case of models other than W@Au_{12}CO, although bridge and hollow sites are also evident, they are still energetically lower than the on-top site by at least 18 kcal mol^{-1}. Furthermore, looking at

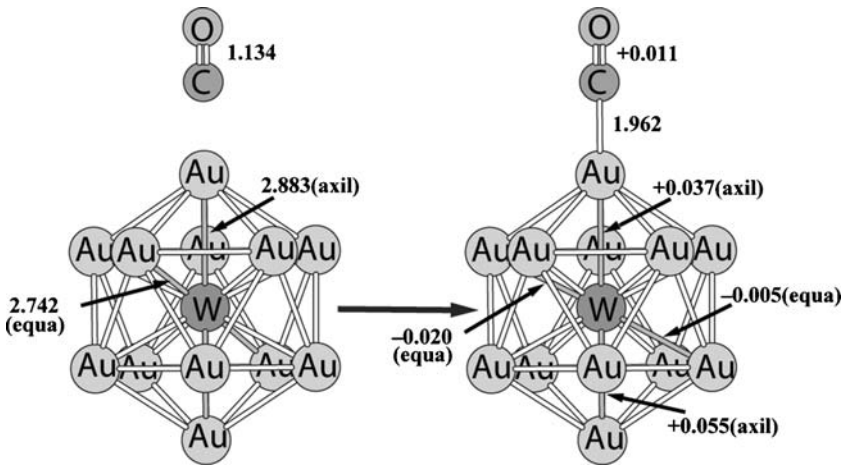

Fig. 3 Geometry influence of the ligand in W@Au_{12}CO complexes. The most important geometrical parameters are given in Ångstroms. + and − indicate increase/decrease in bond lengths, respectively, between before and after bonding with the CO ligand

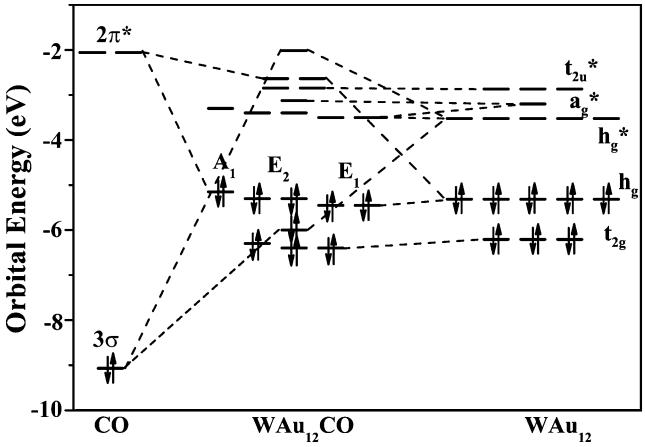

Fig. 4 Orbital correlation diagrams of CO, W@Au_{12} and W@Au_{12}CO

Table 2 Optimized geometric structures of W@Au_{12}AE complexes, free fragments of AE and W@Au_{12}, and the change from free to bonded states (ΔR). *R* Atomic distance (Å)

	NO^+	CO	BF	CN^-	BO^-
R_{A-E}	1.147	1.145	1.279	1.171	1.231
$R_{A-E(free)}$	1.066	1.134	1.272	1.181	1.244
ΔR_{A-E}	+0.082	+0.011	+0.007	–0.010	–0.013
$R_{Au-W(axial)}$	2.708	2.779	2.849	2.797	2.869
$\Delta R_{Au-W(axial)}$	–0.030	+0.041	+0.111	+0.059	+0.131
$R_{Au-W(equatorial)}$	2.751	2.748	2.747	2.747	2.751
R_{Au-A}	1.945	1.962	1.940	2.035	2.051
BE	88.18	29.22	51.65	76.20	91.59

W@Au_{12}CO, we notice that its bridge and hollow adsorption energies are especially low. It means that CO binds only to the on-top site of W@Au_{12}.

Combination effects on geometries of W@Au_{12} and CO

Since the on-top configuration is the most favorable for W@Au_{12}–CO, and the orbital characters of the AE diatomics are similar to those of CO [21, 22], we chose W@Au_{12}CO as an example to illustrate how exactly AE interacts with the metal cluster. In order to examine the on-top site W@Au_{12}CO model, the calculated geometries of free CO, W@Au_{12}(I_h) and W@Au_{12}CO are depicted in Fig. 3. The relative bond lengths give information about changes in the structures caused by the complexation process. For CO in the complex, we note an increase in bond length (1.1 pm) with respect to the free ligand. Our result is consistent with the study of first-row transition metal carbonyl complexes by Sherwood et al. [50]. The extension of the C–O bond can be explained by the antibonding character of CO's 3σ* HOMO and 2π* LUMOs. As a result of calculation, the Mulliken negative overlap population of the 2π* LUMOs is −0.37, which is much larger than that of the 3σ HOMO, which is −0.13. Our calculations are consistent with those of Wada et al. [51]. The 3σ* HOMO can be referred to as a non–bonding orbital. That is why σ-donation does not necessarily result in increased bond distance values [52]. Thus, the Au→CO σ-back-donation taking place in the C–O 2π*-antibonding orbitals contributes more effectively to extension of the CO bond than σ-donation.

From Fig. 3, it can be seen that the axial Au–W bonds are significantly longer than the equatorial bonds. It becomes evident that the C→W@Au_{12} σ-donation transfers into the empty a_1* antibonding LUMOs, forming the HOMO–1 of the complex (see Fig. 4). The σ-donation orbital a_1 is composed mainly of Au $5d_{z^2}$ and 6s. The HOMO 3σ* of CO interacts directly with the hybridized orbital ($5d_{z^2}$ and 6s) of Au1. The interaction forms an antibonding MO, which, according to Hoffman's rule [53], should have a higher amplitude on the more electropositive atom Au1 toward atom W. Therefore, the σ electrons from CO, in fact, transfer into the antibond between Au1 and W and yields longer bond length. Similarly, electrons transferring into the $5d_{z^2}$ AO of W finally result in a longer distance between W and Au2.

Geometric structures of W@Au_{12}AE (AE=NO^+, CO, BF, CN^-, or BO^-)

This section compares various ligands that are isoelectronic to CO. We will see how much they can differ, especially

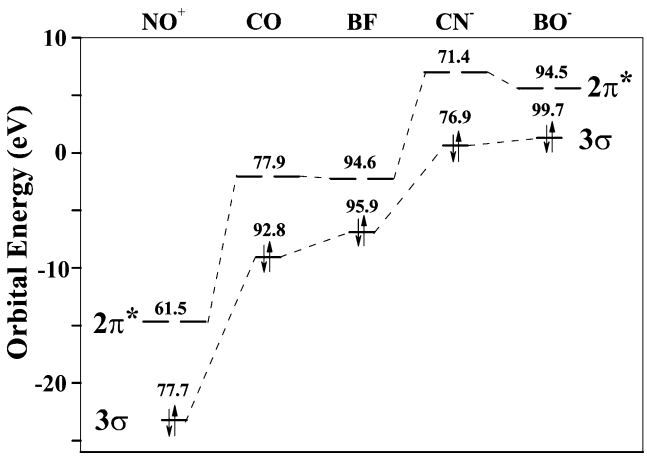

Fig. 5 Valence orbital energies (in eV) of AE systems NO^+, CO, BF, CN^-, and BO^-. The orbital components from the 2p of A are indicated above each orbital level

Table 3 Partial charges (q) of the free ligands AE and the complexes W@Au_{12}AE and differences in the partial charges between the free and bonded ligand[a,b]

Model	q	NO^+	CO	BF	CN^-	BO^-
Free ligand	q (A)	0.785	0.47	0.514	–0.265	–0.04
W@Au_{12}AE	Δq (A)	–0.725	–0.103	+0.112	+0.107	+0.445
	Δq_σ (A)	+0.044	+0.219	+0.411	+0.360	+0.619
	Δq_π (A)	–0.769	–0.322	–0.299	–0.253	–0.174
	$-\Delta q_\sigma$ (A)/Δq_π (A)	0.06	0.68	1.37	1.42	3.55

[a] Partial charges were derived from the NBO analysis at PW91PW91/SDD for the metals, 6–31 g* for the main–group elements

[b] + or − before the numbers indicates increase or decreases in electronic charges

when charge effects come into play (as for NO^+, CN^-, and BO^-). Moreover, as well as the analogies amongst AE ligands, we also compare AE to PH_3, one of the most ubiquitous and well–studied ligands.

The optimized characteristics of the series complexes are summarized in Table 2. It is interesting to note that the axial Au–W bond lengths in W@Au_{12}BF and W@Au_{12} BO^- are significantly longer than those in the other complexes, although the metal–ligand interaction is not very strong in W@Au_{12}BF (BE=51.65 kcal mol^{-1}) compared with W@$Au_{12}NO^+$ (88.18 kcal mol^{-1}) and W@$Au_{12}CN^-$ (76.20 kcal mol^{-1}). We also note that W@$Au_{12}NO^+$ has the shortest axial Au–W bond. The results can be explained by the electronic structures of the ligands. Figure 5 displays the valence orbital energies of the AE diatomics. Above each level the percentage the 2p of A is indicated. We found that boron ligands have a larger percentage of B atom 2p on the frontier orbitals. This is because the 2p energy of atom B is higher than that of atom C, according to Hoffman's rule [53], which should lead to a relatively larger orbital amplitude at atom B and larger overlaps with the relevant W@Au_{12} frontier orbitals as well. As a consequence, the increased interaction with the W@Au_{12} fragment results in increased amplitude of orbitals on atom Au1, finally causing extension of the axial Au–W distances in the cluster. By contrast, NO^+ has a relatively small amplitude at N and a very low energy of the σ HOMO. This leads to a poorer overlap with the metal fragment and results in a much shorter Au–W bond distance.

Next, we considered the intra-ligand bond lengths of the series complexes. As noted in Table 2, the N–O, C–O and B–F bonds are extended when attached to the metal cluster, while the C–N, B–O bonds are shortened. To the best of our knowledge, CO bonds to a transition–metal center involve two distinct charge–transfer interactions: σ-donation and π-back-donation. These two opposing actions affect A–E bond length. Table 3 presents the NBO analysis of AE groups in the complexes and as free molecules. It becomes evident that the $-\Delta q_\sigma$(A)/Δq_π(A) values change less with increasing $\Delta R_{A\text{-}E}$, the A–E bond length change from free to bonded state. The larger percent of $-\Delta q_\pi$ indicates that more π electrons transfer from the occupied h_g HOMO orbital of the W@Au_{12} fragment to the antibonding 2π* orbital of AE, which has the effect of extending the A–E bonds. Conversely, the increase of Δq_σ contributes to shortening the distance between A and E. But we should keep in mind that, in addition to electron transfer, the negative overlap characters of the ligands' frontier orbitals are also very important. A large negative value indicates that the orbital is in an antibonded state. Thus, when electrons get into an orbital with a large negative overlap, bond length will increase. Boron ligands have higher Mulliken overlap populations than CO in corresponding orbitals; details can be found in a former study [22].

The NBO analysis also gives us some interesting information. As noted in Table 3, the overall charge transfer of CO is quite close to zero, which indicates that CO still

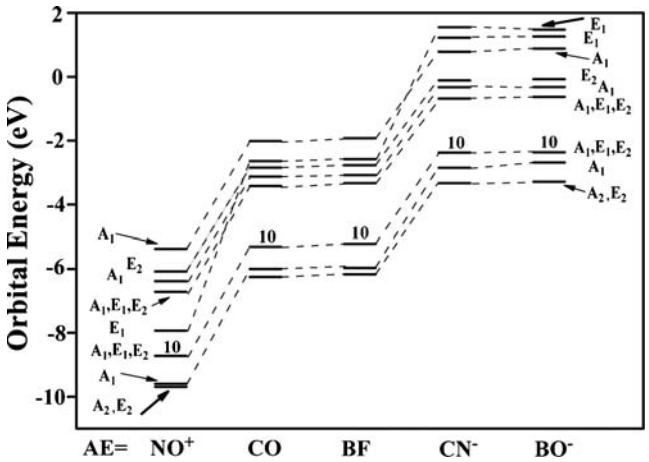

Fig. 6 Orbital level diagram of W@Au_{12}AE (occupations as indicated)

Table 4 Decomposition bond energy (in kcal mol^{-1}) of W@Au_{12}–AE

	NO^+	CO	BF	CN^-	BO^-
ΔE_{prep}	9.49	0.77	1.63	1.16	2.39
ΔE_{pauli}	137.07	193.99	270.14	196.73	282.46
ΔE_{elstat}	–45.30	–139.86	–222.22	–183.84	–280.35
ΔE_{st}	91.76	54.13	47.92	12.89	2.11
ΔE_{orb}	–189.43	–84.12	–101.2	–90.25	–96.09
$\Delta E_{orb(\sigma)}$	–26.38	–46.42	–57.23	–72.78	–79.03
$\Delta E_{orb(\pi)}$	–159.93	–37.25	–43.22	–15.52	–14.87
$\Delta E_{orb(rest)}$	–3.13	–0.45	–0.75	–1.95	–2.19
$\Delta E_{elstat}/\Delta E_{orb}$	0.24	1.66	2.2	2.04	2.92
$\Delta E_{orb(\sigma)}/\Delta E_{orb(\pi)}$	0.16	1.25	1.32	4.69	5.32
BE(WAu_{12}–AE)	88.18	29.22	51.65	76.2	91.59

remains electrically neutral. This feature makes CO a special ligand, which is important in stabilizing the metal cluster. As for the other AE ligands, the atomic partial charges suggest that NO^+ is overall electron acceptor, while BF, CN^- and BO^- are overall electron donors.

Molecular orbitals

A molecular orbital diagram of W@Au_{12}AE (AE=NO^+, CO, BF, CN^-, or BO^-) is shown in Fig. 6. All bonding orbitals have been earmarked separately with σ and π signs. The HOMOs are indicated by the number of electron occupancies they have. As a result of combination with AE ligands, both the degenerate hg HOMO and the hg* LUMO of W@Au_{12} begin to split into three energy levels, with A_1, E_1 and E_2 symmetry, respectively. Even though there are energy differences among these orbitals, these are relatively small and can be neglected in comparison to the relative large HOMO–LUMO gaps.

In Fig. 6, we notice that the orbitals take a large leap from W@$Au_{12}NO^+$ to W@Au_{12}CO. Meanwhile there is also another orbital energy gap from W@Au_{12}BF to W@$Au_{12}CN^-$. This scheme is consistent with the energy levels of the orbitals of the corresponding ligands, as depicted in Fig. 5, since the AE diatomics display similar trends from NO^+ to BO^-. This suggests that, for the complexes, the exact energies of the frontier orbitals are influenced strongly by the nature of the ligands they contain.

Bond energy analysis

In this part, we will calculate the bond energies between AE and W@Au_{12}, and also the A–E bond energies. An ETS analysis will be presented. An introduction to ETS analysis and the methods of calculation of BE(W@Au_{12}–AE) can be found in the Methods. Here, we define the bond energy between A and E as the following:

$$\mathrm{BE}(\mathrm{W@Au_{12}} - \mathrm{AE}) = -\left(E_{\mathrm{W@Au12AE}} - E_{\mathrm{W@Au12}} - E_{\mathrm{AE}}\right) \quad (4)$$

$$\mathrm{BE}(\mathrm{W@Au_{12}A} - \mathrm{E}) = -\left(E_{\mathrm{W@Au12AE}} - E_{\mathrm{W@Au12A}} - E_{\mathrm{E}}\right) \quad (5)$$

The energy decompositions are listed in Table 4. The results for negative, neutral and positive ligands will be discussed separately. The calculated metal–ligand bond energies show that, among the negatively charged ligands, the Au–BO^- bond is thermodynamically more stable than the corresponding bond of W@$Au_{12}CN^-$ due to its greater electrostatic attraction (ΔE_{ele}). For the neutral complexes, the Au–BF bond is much stronger with respect to the Au–CO bond, but they are both weaker than those of the negative ligands. The bond to the positive NO^+ is also stronger than that to CO or BF, although the bond strength is a little weaker than that of BO^-.

Table 5 Intra-ligand bond energies (BE) (in kcal mol^{-1}) in the free and bonded states. Δ Change from free to bonded structures. Bond length R (in Å)

	NO^+	CO	BF	CN^-	BO^-
BE(W@Au_{12}A–E)	180.4	255.02	179.93	316.69	260.89
BE(A–E) (free)	303.82	279.83	197.54	291.96	238.53
ΔBE(A–E)	–123.42	–24.81	–17.61	24.73	22.36
$\Delta R_{A\text{-}E}$	0.082	0.011	0.007	–0.010	–0.013

Table 6 The highest occupied molecular orbital (HOMO)–lowest unoccupied molecular orbital (LUMO) energy gap of $W@Au_{12}AE$ and difference of the HOMO–LUMO gap between the complex and $W@Au_{12}$. Energies are given in eV. The LUMO–HOMO gap of free $W@Au_{12}$ is 1.787 eV

	NO^+	CO	BF	CN^-	BO^-
LUMO	–7.940	–3.459	–3.363	–0.719	–0.659
HOMO	–8.688	–5.247	–5.060	–2.260	–2.020
LUMO–HOMO gap	0.748	1.788	1.697	1.541	1.361
Δgap	–1.039	+0.001	–0.090	–0.246	–0.426

The orbital interactions ΔE_{orb} can be divided into $\Delta E_{orb(\sigma)}$, $\Delta E_{orb(\pi)}$, and the remainder $\Delta E_{orb(rest)}$. From Table 4, we can see that the term ΔE_{prep} is very small except for $W@Au_{12}NO^+$. The term ΔE_{prep} of $W@Au_{12}NO^+$ is relatively large because the deformation of the fragment geometries from free structures to the geometries in the complexes is larger than for the other complexes. The most important information about the ionic/covalent character of the bond is given by the ratio $\Delta E_{elstat}/\Delta E_{orb}$. The positive charge reduces the polarization of Au–N molecular orbitals, which lead to the most covalent Au–A bond. In contrast, the polarized boron ligands tend to have a more electrostatic interaction with the metal cluster. Although the $\Delta E_{orb(\pi)}$ term descends along the series, we should consider the ratio of the σ-donation and π-back-donation, which is a more meaningful indicator of the π-acceptor strength of the ligands. The $\Delta E_{orb(\sigma)}/\Delta E_{orb(\pi)}$ values exhibit a clear increase along the series, which is consistent with the donor/acceptor charge ratio in Table 3.

The bond energies between A and E are listed in Table 5. It is clear that the A–E bond lengths and bond energies have an inverse relationship. All the complexes whose A–E bond distances increase compared to those in the free ligands will be accompanied by stronger bond strengths, and vice versa. It is interesting that the bond strengths of NO^+, CO and BF become weaker than of their free states when bonded to the $W@Au_{12}$ cluster. In this sense, these molecules may be more active, and may break their bonds more easily after bonding to gold clusters.

Kinetic stability

The kinetic stability of a molecule has a crucial influence on its synthetic accessibility and ease of isolation. In order for a molecule to be isolable, it must be not only thermodynamically but also kinetically stable. It is well known that the energy gap between the highest occupied molecular orbital (HOMO) and the lowest unoccupied molecular orbital (LUMO) is an indicator of kinetic stability [54–57]. It is difficult for electrons to transfer from an occupied orbital to an unoccupied orbital if the cluster has a wide HOMO–LUMO gap. Reversely, a small HOMO–LUMO gap suggests a low kinetic stability.

Table 6 indicates that $W@Au_{12}CO$ has the widest HOMO–LUMO gap among the six complexes, with $W@Au_{12}PH_3$ second. However, we found that, except for $W@Au_{12}CO$, the HOMO–LUMO gaps of all the other complexes are narrower than that of $W@Au_{12}$, which means that these complexes make the cluster kinetically unstable. Among them, $W@Au_{12}NO^+$ has the lowest kinetic stability, since its HOMO–LUMO gap is very small. Moreover, the positive charge on NO^+ causes it to suffer nucleophilic attack rather easily, which makes $W@Au_{12}NO^+$ quite an unstable compound.

Summary and conclusions

The present DFT calculations have provided the following interpretations of AE ligands on the $W@Au_{12}$ cluster.

(1) The optimized geometries and bond dissociation energies of hollow, bridge and on-top sited complexes prove that the on-top configuration is favored by all five ligands (NO^+, CO, BF, CN^-, BO^-) on the $W@Au_{12}$ fragment. Moreover, A of AE should be the ligating atom in all ligands investigated.

(2) NO^+, CO, BF, CN^- and BO^- have different effects on the geometry of the metal cluster. BF and BO^- have an inclination to drag the axial Au–W bond distance significantly. On the other hand, the axial Au–W bond length is shortened when the $W@Au_{12}$ fragment is combined with NO^+. Furthermore, the differences in the intra-ligand bond lengths in complexes between those in free ligands decrease along the series.

(3) The frontier orbitals of $W@Au_{12}AE$ are similar to those of $W@Au_{12}$ fragment in shape, although their energy levels are affected by relevant interaction orbitals of the AE ligands. These energy alterations may be a key factor in activating or protecting the metal cluster.

(4) The donor/acceptor ratio derived from the transfer of electrons and the ETS suggests that σ-donation strength increases steadily from NO^+ to BO^-. Thus, we conclude that, with smaller ratio, ligands are prone to take in electrons on to the AE's $2\pi^*$ antibonding orbital and the A–E bonds are reduced in strength.

(5) Except for CO, all the other $W@Au_{12}AE$ have smaller HOMO–LUMO gaps than that of $W@Au_{12}$, which means they are kinetically unstable.

Acknowledgments We acknowledge financial support by the National Nature Science Foundation of China (No. 20573074) and the Specialized Research Fund for the Doctoral Program of Higher Education of China (No. 20040248017).

References

1. Bond GC, Thompson DT (1990) Catal Rev Sci Eng 41:319–388
2. Hashmi ASK, Hutchings GJ (2006) Angew Chem Int Ed 45:7896–7936
3. Bond GC, Sermon PA, Webb G, Buchanan DA, Wells PB (1973) J Chem Soc Chem Commun 13:444–445
4. Haruta M (2005) Nature 437:1098–1099
5. Haruta M, Kobayashi T, Sano H, Yamada N (1987) Chem Lett 16:405–408
6. Hayashi T, Tanaka K, Haruta M (1998) J Catal 178:566–575
7. Solsona B, Conte M, Cong Y, Carley A, Hutchings G (2005) Chem Commun 18:2351–2353
8. Cunningham DAH, Vogel W, Kageyama H, Tsubota S, Haruta MJ (1998) J Catal 177:1–10
9. Garzón IL, Michaelian K, Beltrán MR, Posada-Amarillas A, Ordejón P, Artacho E, Sánchez-Portal D, Soler JM (1998) Phys Rev Lett 81:1600–1603
10. Wang JL, Wang GH, Zhao JJ (2002) Phys Rev B 66:035418
11. Oviedo J, Palmer RE (2002) J Chem Phys 117:9548–9551
12. Pyykkö P, Runeberg N (2002) Angew Chem Int Ed 41:2174–2176
13. Pyykkö P (1988) Chem Rev 88:563–594
14. Scherbaum F, Grohmann A, Huber B, Krüger C, Schmidbaur H (1988) Angew Chem Int Ed Engl 27:1544–1546
15. Pyykkö P (2006) J Org Chem 691:4336–4340
16. Autschbach J, Hess BA, Johansson MP, Neugebauer J, Patzschke M, Pyykkö P, Reiher M, Sundholm D (2004) Phys Chem Chem Phys 6:11–22
17. Li X, Kiran B, Li J, Zhai HJ, Wang LS (2002) Angew Chem Int Ed 41:4786–4789
18. Werner H (1990) Angew Chem 102:1109–1121
19. Werner H (1990) Angew Chem Int Ed Engl 29:1077–1089
20. Ehlers AW, Dapprich S, Vyboishchikov SF, Frenking G (1996) Organometallics 15:105–117
21. Radius U, Bickelhaupt FM, Ehlers AW, Goldberg N, Hoffmann R (1998) Inorg Chem 17:1080–1090
22. Ehlers AW, Baerends EJ, Bickelhaupt FM, Radius U (1998) Chem Eur J 4:210–221
23. Fu Q, Saltsburg H, Flytzani-Stephanopoulos M (2003) Science 301:935–938
24. te Velde G, Bickelhaupt FM, Baerends EJ, Guerra CF, van Gisbergen SJA, Snijders JG, Ziegler T (2001) J Comput Chem 22:931–967
25. Bickelhaupt FM, Baerends EJ (2000) Reviews in computational chemistry, vol 15. Wiley-VCH, New York, pp 1–86
26. Vosko SH, Wilk L, Nusair M (1980) Can J Phys 58:1200–1211
27. Perdew JP, Wang Y (1992) Phys Rev B 45:13244–13249
28. Perdew JP, Chevary JA, Vosko SH, Jackson KA, Pederson MR, Singh DJ, Fiolhais C (1992) Phys Rev B 46:6671–6687
29. van Lenthe E, Baerends EJ, Snijders JG (1994) J Chem Phys 101:9783–9792
30. van Lenthe E, van Leeuwen R, Baerends EJ, Snijders JG (1996) Int J Quantum Chem 57:281–293
31. van Lenthe E, Snijders JG, Baerends EJ (1996) J Chem Phys 105:6505–6516
32. van Lenthe E, Ehlers A, Baerends EJ (1999) J Chem Phys 110:8943–8953
33. van Lenthe E, Baerends EJ (2003) J Comput Chem 24:1142–1156
34. Rosen A, Lindgren I (1968) Phys Rev 176:114–125
35. Reed AE, Weinstock RB, Weinhold F (1985) J Chem Phys 83:735–746
36. Reed AE, Curtiss LA, Weinhold F (1988) Chem Rev 88:899–926
37. Foster JP, Weinhold F (1980) J Am Chem Soc 102:7211–7218
38. Brunck TK, Weinhold F (1979) J Am Chem Soc 101:1700–1709
39. Reed AE, Weinhold F (1985) J Chem Phys 83:1736–1740
40. Weinhold F, Carpenter JE (1988) The structure of small molecules and ions. Plenum, New York
41. Frisch MJ, Trucks GW, Schlegel HB, Scuseria GE, Robb MA, Cheeseman JR, Montgomery JA Jr, Vreven T, Kudin KN, Burant JC, Millam JM, Iyengar SS, Tomasi J, Barone V, Mennucci B, Cossi M, Scalmani G, Rega N, Petersson GA, Nakatsuji H, Hada M, Ehara M, Toyota K, Fukuda R, Hasegawa J, Ishida M, Nakajima T, Honda Y, Kitao O, Nakai H, Klene M, Li X, Knox JE, Hratchian HP, Cross JB, Bakken V, Adamo C, Jaramillo J, Gomperts R, Stratmann RE, Yazyev O, Austin AJ, Cammi R, Pomelli C, Ochterski JW, Ayala PY, Morokuma K, Voth GA, Salvador P, Dannenberg JJ, Zakrzewski VG, Dapprich S, Daniels AD, Strain MC, Farkas O, Malick DK, Rabuck AD, Raghavachari K, Foresman JB, Ortiz JV, Cui Q, Baboul AG, Clifford S, Cioslowski J, Stefanov BB, Liu G, Liashenko A, Piskorz P, Komaromi I, Martin RL, Fox DJ, Keith T, Al-Laham MA, Peng CY, Nanayakkara A, Challacombe M, Gill PMW, Johnson B, Chen W, Wong MW, Gonzalez C, Pople JA (2003) Gaussian 03, Revision B3. Gaussian Inc, Pittsburgh, PA
42. Ziegler T, Rauk A (1977) Theor Chim Acta 46:1–10
43. Ziegler T, Rauk A (1979) Inorg Chem 18:1558–1565
44. Ziegler T, Rauk A (1979) Inorg Chem 18:1755–1759
45. Ziegler T, Tschinke V, Becke A (1987) J Am Chem Soc 109:1351–1358
46. Ziegler T, Tschinke V, Ursenbach C (1987) J Am Chem Soc 109:4825–4837
47. Li J, Schreckenbach G, Ziegler T (1995) J Am Chem Soc 117:486–494
48. Dewar MJS (1951) Bull Soc Chim Fr 18:C79
49. Long J, Qiu YX, Chen XY, Wang SG (2008) J Phys Chem C 112:12646–12652
50. Sherwood DE, Hall MB (1983) Inorg Chem 22:93–100
51. Wada T, Nishio S, Yada T, Hayashi S (1998) Appl Organometal Chem 12:419–426
52. Goldman AS, Krogh-Jespersen K (1996) J Am Chem Soc 118:12159–12166
53. Hoffmann R (1971) Acc Chem Res 4:1–9
54. Manolopoulos DE, May JC, Down SE (1991) Chem Phys Lett 181:105–111
55. Hess BA Jr, Schaad LJ (1971) J Am Chem Soc 93:2413–2416
56. Schmalz TG, Seitz WA, Klein DJ, Hite GE (1988) J Am Chem Soc 110:1113–1127
57. Zhou Z, Parr RG (1989) J Am Chem Soc 111:7371–7379